GEOLOGICA CARPATHICA, OCTOBER 2013, 64, 5, 409–416 doi: 10.2478/geoca-2013-0028

Correlation between Cu mineralization and major faults using multifractal modelling in the Tarom area (NW Iran)

REZA NOURI[1]✉, MOHAMMAD REZA JAFARI[1], MEHRAN ARIAN[2], FARANAK FEIZI[3] and PEYMAN AFZAL[3,4]

[1]Department of Geology, North Tehran Branch, Islamic Azad University, Tehran, Iran; ✉reza_noor2002@yahoo.com
[2]Department of Geology, Science and Research Branch, Islamic Azad University, Tehran, Iran
[3]Department of Mining Engineering, South Tehran Branch, Islamic Azad University, Tehran, Iran
[4]Camborne School of Mines, University of Exeter, Penryn, United Kingdom

(Manuscript received January 4, 2013; accepted in revised form June 5, 2013)

Abstract: The Tarom 1 : 100,000 sheet is located within the Cenozoic Tarom-Hashtjin volcano-plutonic belt, NW Iran. Reconstruction of the tectonic and structural setting of the hydrothermal deposits is fundamental to predictive models of different ore deposits. Since fractal/multifractal modelling is an effective instrument for separation of geological and mineralized zones from background, therefore Concentration-Distance to Major Fault (C-DMF) fractal model and distribution of Cu anomalies were used to classify Cu mineralizations according to their distance to major faults. Application of the C-DMF model for the classification of Cu mineralization in the Tarom 1 : 100,000 sheet reveals that the main copper mineralizations have a strong correlation with their distance to major faults in the area. The distances of known copper mineralizations having Cu values higher than 2.2 % to major faults are less than 10 km showing a positive correlation between Cu mineralization and tectonic events. Moreover, extreme and high Cu anomalies based on stream sediments and lithogeochemical data were identified by the Number-Size (N-S) fractal model. These anomalies have distances to major faults less than 10 km and validate the results derived via the C-DMF fractal model. The C-DMF fractal modelling can be utilized for the reconnaissance and prospecting of magmatic and hydrothermal deposits.

Key words: Multifractal, stream sediment, lithogeochemical, copper mineralization, Concentration-Distance to Major Fault (C-DMF).

Introduction

A geochemical anomaly occurs by various natural processes related to different geological events (e.g. tectonics, mineralization: Zhao 1999; Cheng 2007; Cheng & Agterberg 2009; Wang et al. 2012). It may reveal important changes either in geological characteristics and/or mineralization processes. Separation of geochemical anomalies from background is an important operation in mineral exploration. However, recognition and delineation of the anomalies to predict the occurrence of mineral deposits need the knowledge of geo-anomaly according to mineralization types, grade distributions and geneses and knowledge of advanced methods for their quantitative mapping. In the past decades, two basic methods have been commonly utilized to analyse geochemical exploration data consisting of frequency analysis and spatial analysis (Grunsky & Smee 1999; Harris et al. 2000; Xu & Cheng 2001; Pereira et al. 2003; Wang et al. 2012). Separation of anomalies from background is the most significant purpose of geochemical exploration operations especially for metallic ore deposits. Stream sediment and lithogeochemical studies are essential for prospecting different types of ore deposits (Hawkes & Webb 1979). Several methods are used for geochemical data interpretation and modelling such as classical statistics (e.g. Tukey 1977; Hawkes & Webb 1979; Reimann et al. 2005), fractal and multifractal modelling (Cheng et al. 1994; Agterberg et al. 1996; Cheng 1999; Li et al. 2003; Zuo et al. 2009; Afzal et al. 2010) and singularity modelling (Cheng 2007; Wang 2012). Fractal theory has been established by Mandelbrot (1983) as an important non-Euclidean branch in geometry. Several methods and models have been proposed and developed based on fractal geometry for application in the geosciences since the 1980s (Agterberg et al. 1993; Sanderson et al. 1994; Cheng 1999; Turcotte 1997, 2002; Gonçalves et al. 2001; Monecke et al. 2005; Gumiel et al. 2010; Afzal et al. 2011; Zuo 2011; Sadeghi et al. 2012; Yasrebi et al. 2013).

The aim of structural analysis applied to mineralization is to identify what deformation influenced the increase or decrease of permeability in rocks, both spatially and over time. There is a positive correlation between tectonic and hydrothermal mineralization. Such understanding can contribute to predictive models of deposit geometry and extensions to known deposits, and also to exploration models (Craw & Campbell 2004; Micklethwaite et al. 2010). The purpose of this study is to classify Cu mineralizations according to their distance to major faults by Concentration-Distance to Major Fault (C-DMF) fractal model and distribution of Cu anomalies by using a multifractal method, in the 1 : 100,000 Tarom sheet, NW Iran.

Geological setting of the Tarom 1 : 100,000 sheet

The Tarom 1 : 100,000 sheet, located in Zanjan Province NW Iran, was chosen as the study area because there are Cu-Au polymetallic deposits which are part of the Tarom polyme-

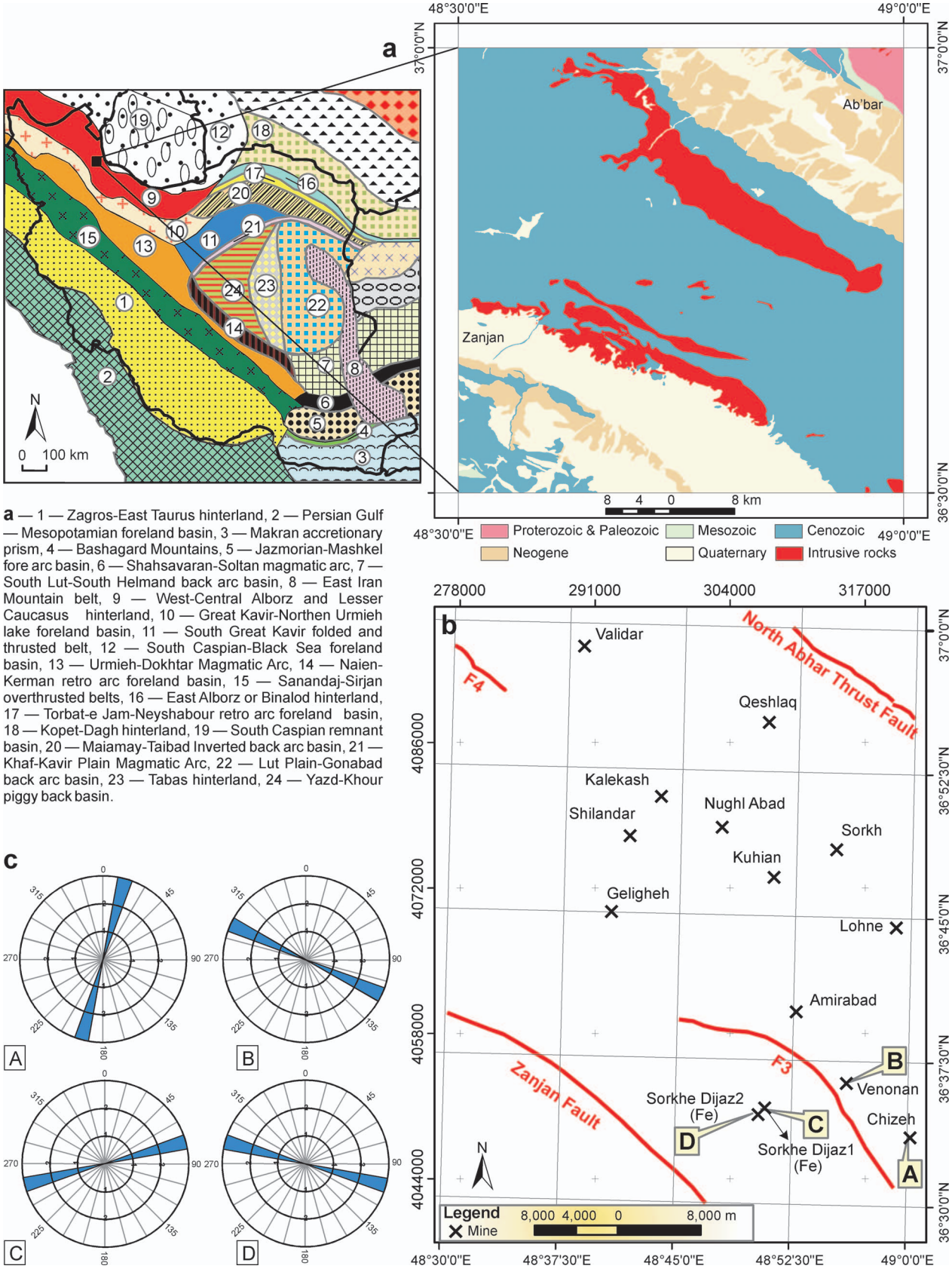

a — 1 — Zagros-East Taurus hinterland, 2 — Persian Gulf — Mesopotamian foreland basin, 3 — Makran accretionary prism, 4 — Bashagard Mountains, 5 — Jazmorian-Mashkel fore arc basin, 6 — Shahsavaran-Soltan magmatic arc, 7 — South Lut-South Helmand back arc basin, 8 — East Iran Mountain belt, 9 — West-Central Alborz and Lesser Caucasus hinterland, 10 — Great Kavir-Northen Urmieh lake foreland basin, 11 — South Great Kavir folded and thrusted belt, 12 — South Caspian-Black Sea foreland basin, 13 — Urmieh-Dokhtar Magmatic Arc, 14 — Naien-Kerman retro arc foreland basin, 15 — Sanandaj-Sirjan overthrusted belts, 16 — East Alborz or Binalod hinterland, 17 — Torbat-e Jam-Neyshabour retro arc foreland basin, 18 — Kopet-Dagh hinterland, 19 — South Caspian remnant basin, 20 — Maiamay-Taibad Inverted back arc basin, 21 — Khaf-Kavir Plain Magmatic Arc, 22 — Lut Plain-Gonabad back arc basin, 23 — Tabas hinterland, 24 — Yazd-Khour piggy back basin.

Fig. 1. a — The physiographic-tectonic zoning map of Iran's sedimentary basins (Arian 2011). Geological map of studied area based on 1:100,000 geological map of Tarom (Amini et al. 1969) is shown in the square box. **b** — Major fault map of the study area with mine potentials. **c** — Rose diagrams of main veins in selected point on fig. 1b.

tallic zone that lie in the Alpine-Himalayan Mountain Range (Fig. 1). There are two great intrusive masses in the same direction of the volcanic rocks and other small outcrops within basic, acidic and intermediate compositions (Mousavi 2012). One of the noticeable features of magmatic highlands in the study area is the presence of large granitic and granodioritic bodies, which have intruded into the Eocene pyroclastic rocks (Karaj Formation). These represent post-Eocene intrusive bodies of the Pyrenean orogenic phase intruding along the direction of deep NW-SE major fault zones in the Tarom Mountain Range (Table 1 and Fig. 2). Alteration halos in Eocene volcaniclastic rocks are one of the characteristic consequences of these intrusive events. There are sub-volcanic intrusions with silicic, argillic, propylitic and sericitic hydrothermal alteration. Similar plutons and intrusions are common in the Alborz–Azarbaijan structural zone of Iran, and it is likely that there are concealed plutons related to this extensive Cenozoic magmatism (Karimzadeh Somarin 2006). The intrusions contain ore minerals of Cu, Pb, Zn, Au, Ag and Fe such as chalcopyrite, chalcocite, malachite, magnetite, galena and sphalerite. Mineralized Cu veins including malachite, chalcocite, bornite and azurite occur in Eocene ignimbrites and tuffs which have similar trends to the major faults in the area, especially NNW-SSE. Mineralization of gold, copper, lead–zinc, and kaolinite are associated with these hydrothermal alteration halos (Azizi et al. 2010).

Table 1: Characterization of the major faults in the Tarom area.

Name	Type	Length (km)	Strike
Zanjan	Thrust — Inverse	32	Zanjan1: N104 Zanjan2: N114 Zanjan3: N123 Zanjan4: N127
North Abhar	Thrust — Inverse	15	Abhar1: N129 Abhar2: N111 Abhar3: N122
F3	Thrust — Inverse	28	F3-1: N97 F3-2: N103 F3-3: N94 F3-4: N107 F3-5: N116 F3-6: N129 F3-7: N153 F3-8: N140
F4	Thrust — Inverse	6.7	F4-1: N114 F4-2: N125 F4-3: N161 F4-4: N117

Tectonic setting

Based on the physiographic-tectonic zoning map of Iran's sedimentary basins (Arian 2011), the dominant structural trend in the Western Central Alborz and Lesser Caucasus province (No. 9) is NW-SE (Fig. 1). It corresponds to a deformed zone (fold and thrust belt) of the Cimmerian miniplate that formed in the northern active margin until the Late

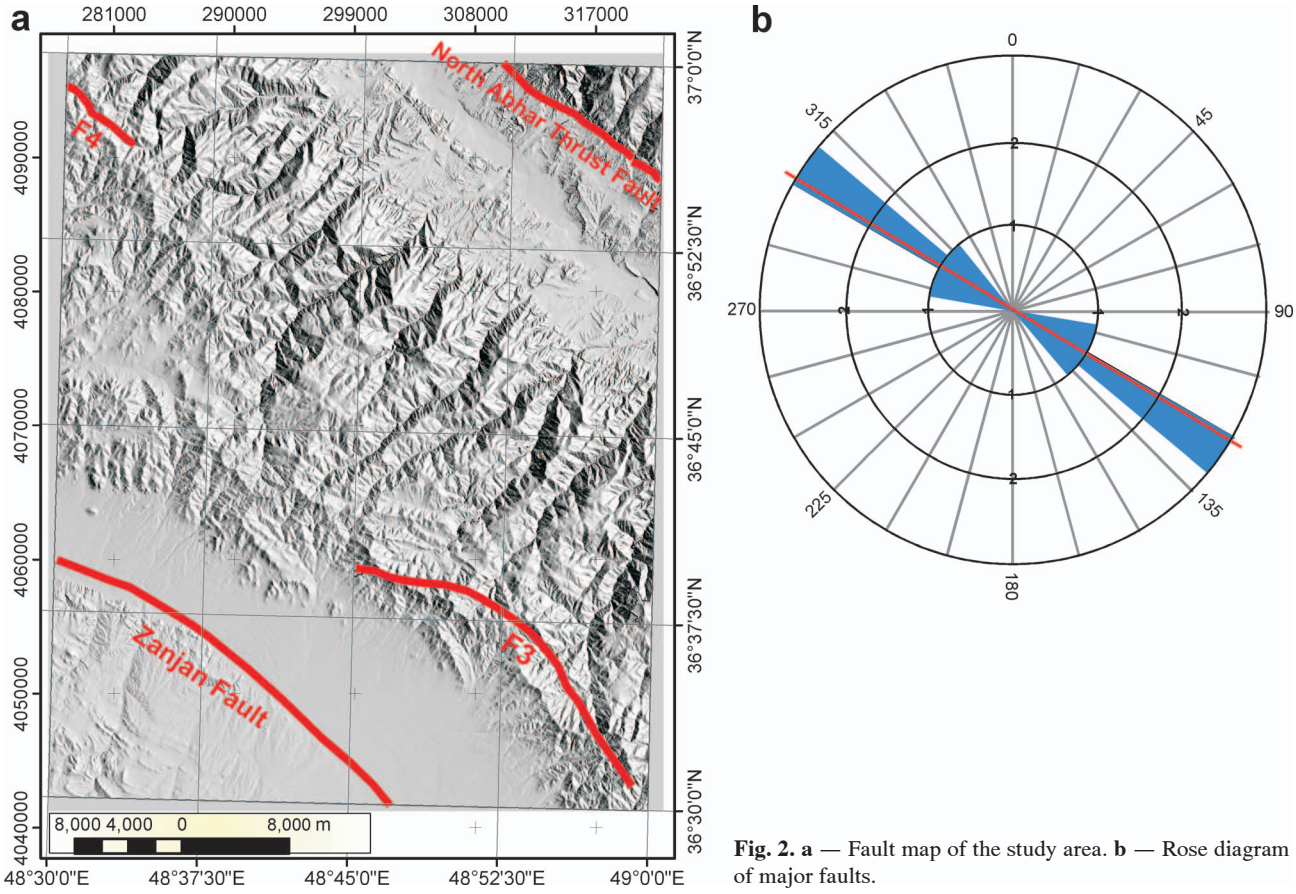

Fig. 2. a — Fault map of the study area. **b** — Rose diagram of major faults.

Triassic. It was subsequently rifted by extension forming a back-arc basin along the Neo-Tethys subduction zone in the south margin of the Cimmerian miniplate. Rift development stopped in the Late Cretaceous and was renewed in the Eocene by spreading of the submarine arc basin of the Neo-Tethys subduction zone. In summary, this hinterland is the result of a magmatic arc spreading system in a back-arc basin setting. Later, the Western Central Alborz and the Lesser Caucasus hinterland were formed by deformation and regional uplift which extended from the south western margin of the Caspian Sea to the south eastern margin of Black Sea. Recently, the Damavand and Sebalan cones were formed by late volcanism related to the final subduction stages of the oceanic slab in the south Caspian Basin toward the south and southwest. Five dominant orogenic phases and four deformational events in the Alborz Mountain building processes were identified by Arian et al. (2011). The first deformation event is from the collision between the Cimmerian and Eurasian plates (Late Triassic) and the remaining ones are from post-collision events and deformation of the sedimentary cover resulting from the shortening and thickening of the passive continental crust north of the Cimmerian miniplate.

Geological structures

There are many geological structures in the fold and thrust belt of West–Central Alborz and Lesser Caucasus province. The dominant structural trend of the main folds and faults (Fig. 1) is NW-SE. The results of the analysis of fractures and veins are presented in Fig. 1. In the northeast of the Tarom sheet, Eocene rock units have been affected by the North Abhar Thrust Fault. Neogene units have also been overlaid by the dark grey shale and sandstone of the Shemshak Formation (Jurassic), which represented an active fault system during the Holocene. The major faults run along the main structural trend in the area (Table 1). The North Abhar Thrust Fault has a length of 15 km and a NW-SE strike with a general dip towards the NE. In the southwest of the Tarom sheet, occurs the Zanjan Fault which has been interpreted as a major thrust fault. The Zanjan inverse/thrust Fault has a length of 32 km and a NW-SE strike with a general dip toward the SW. Towards the southeast of the Tarom sheet, older units including granite porphyry, andesite, and tuff units (Eocene) have been affected by the F3 thrust fault, and a microquartzdiorite porphyry body (Neogene) has intruded along it. The F3 inverse/thrust Fault has a length of 28 km and a NW-SE strike with a general dip toward the NE. Towards the northwest of the Tarom sheet, the F4 thrust fault affected Eocene tuffs and has a length of 6.7 km and a NW-SE strike with a general dip toward the NE.

Materials and methods

Number-size fractal method

The Number-Size (N-S) method, was originally proposed by Mandelbrot (1983) and can be used to describe the distribution of geochemical populations without pre-processing the data. The method indicates that there is a relationship between desirable attributes (e.g. ore elements) and the cumulative number of samples showing those attributes. Based on this model, Agterberg (1995) proposed a multifractal model for the determination of the spatial distributions of giant and super-giant ore deposits. Monecke et al. (2005) used the N-S fractal model to characterize element enrichments associated with metasomatic processes during the formation of hydrothermal ores in the Waterloo massive sulphide deposit, Australia. A power-law frequency model was proposed to describe the N-S relationship according to the frequency distribution of element concentrations and cumulative number of samples with those attributes (Li et al. 1994; Sanderson et al. 1994; Turcotte 1996; Shi & Wang 1998; Zuo et al. 2009). The model is expressed by the following equation (Mandelbrot 1983; Deng et al. 2010):

$$N(\geq\rho) = F\rho^{-D} \quad (1)$$

where ρ denotes element concentration, N(≥ρ) denotes the cumulative number of samples with concentration values greater than or equal to ρ, F is a constant and D is the scaling exponent or fractal dimension of the distribution of element concentrations. According to Mandelbrot (1983) and Deng et al. (2010), log-log plots of N(≥ρ) versus ρ follow straight line segments with different slopes –D each corresponding to different concentration intervals.

Concentration-Distance to Major Fault fractal model

The Concentration-Distance to Major Fault (C-DMF) fractal model is an extension of the N-S model in the study. The model has the following form:

$$DMF(\geq\rho) = F\rho^{-D} \quad (2)$$

where ρ shows element concentration, DMF(≥ρ) indicates cumulative distance from major faults of sampled sites with concentration values greater than or equal to ρ, F is a constant and D is the scaling exponent or fractal dimension of the distribution of element concentrations. Based on this model, metallic mines, deposits and occurrences were classified according to their distance to major faults.

Results and discussion

Application of N-S fractal method in stream sediment

Stream sediment geochemistry was found to be an efficient method for outlining potentially mineralized areas. The silt fraction of alluvial sediments is representative of the geochemistry of the drainage pattern and reduces the "nugget effect" during sampling (Fletcher 1997; Aichler et al. 2008). Once material enters the stream, processes that move sediment also change its texture and geochemical composition. For example, light mineral fractions < 100 μm tend to be swept away in suspension whenever sediment transport occurs. The geochemical consequences of sediment sorting

are not so obvious for elements (e.g. base metals) that are rather uniformly distributed in different components of the sediments. However, sorting has important consequences for elements such as gold, that are present as constituents of rare heavy minerals. Theory and field studies show that enrichment of these elements on the stream bed is most consistent for the fine sand fractions. Concentrations in coarser size fractions become increasingly erratic, in both space and time, depending on local hydraulic conditions. Thus, the finer fractions are better representatives of the geochemistry of the drainage basin and also reduce the nugget effect during sampling (Fletcher 1997).

The analysed samples were sorted in decreasing order of grades from which cumulative numbers were calculated. Finally, the log-log plot was generated for Cu (Fig. 3). Breaking points between straight-line segments in the log-log plot represent threshold values separating sets of samples whose

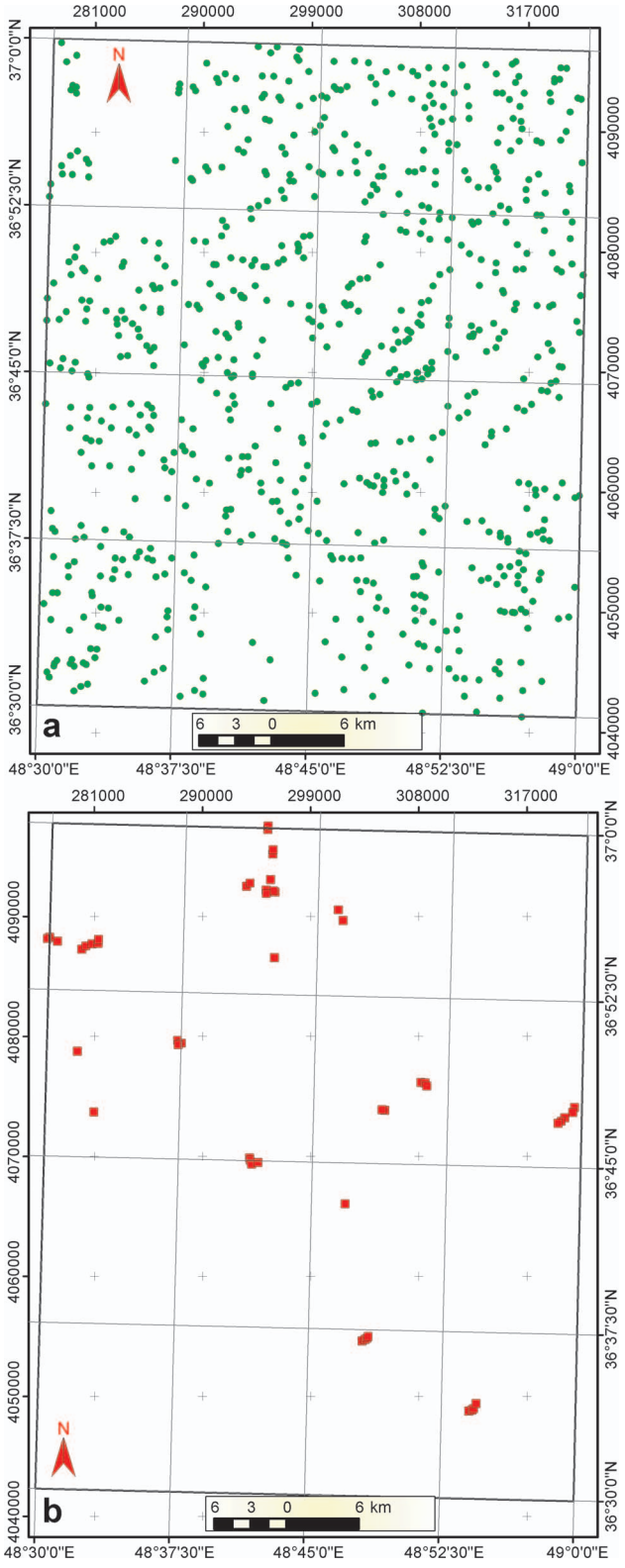

Fig. 3. a — Stream sediment. **b** — Lithogeochemical samples location map of the Tarom sheet.

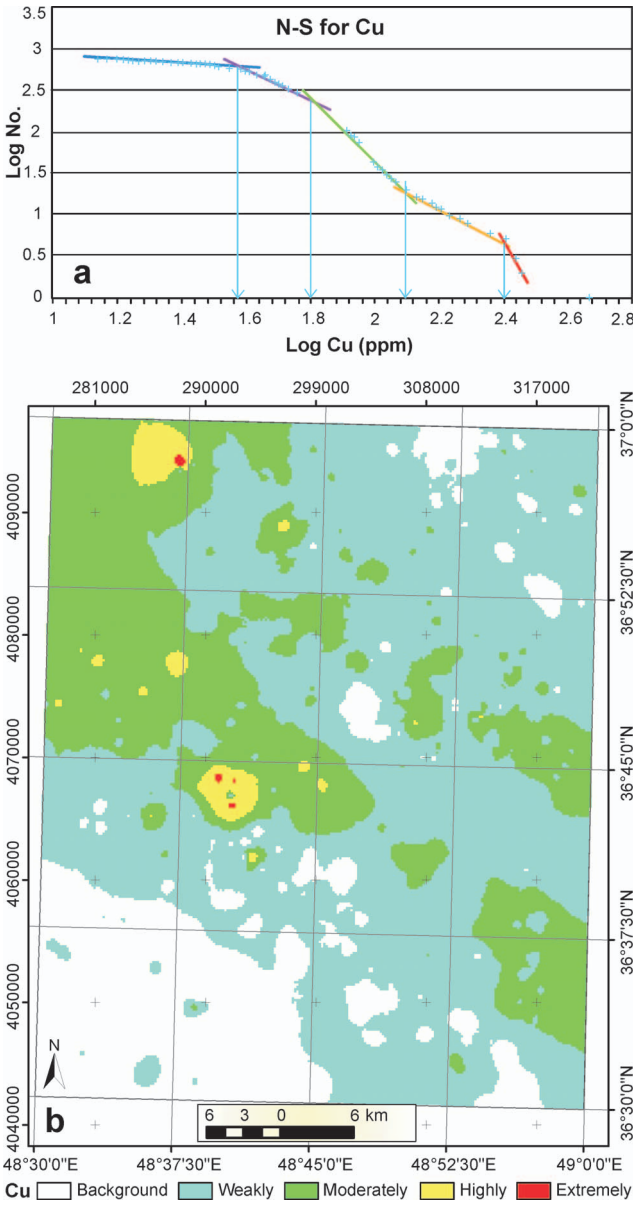

Fig. 4. a — Log-log plots of N-S model for Cu stream sediment data. **b** — Cu stream sediment population distribution map based on the N-S fractal model.

geochemical concentration values outline distinct geological and geochemical processes. Distinct Cu geochemical groups are separated in this log-log plot. Relying on this approach, there are five groups for Cu showing high Cu anomalies with values in excess of 125 ppm.

The area was gridded with cells of 180×180 m^2 for the interpolation of Cu values. The interpolation method used is the Inverse Squared Distance (ISD) which was used for the generation of maps of Cu concentration. This procedure is preferred because it reduces the undesirable smoothing effects caused by Kriging. Kriging also has inherently high truncation errors for the upper and lower boundaries of ore grades. The high values of Cu (≥125 ppm) are located in the central, NW and western parts of the Tarom sheet, as depicted in Fig. 4. The terms of "extreme" and "high" have been utilized in order to explain the high values of Cu anomalies based on lithogeochemical and stream-sediment data, within the area. High and extreme anomalies are shown in last segments (groups) in the log-log plots which have dips near 90°.

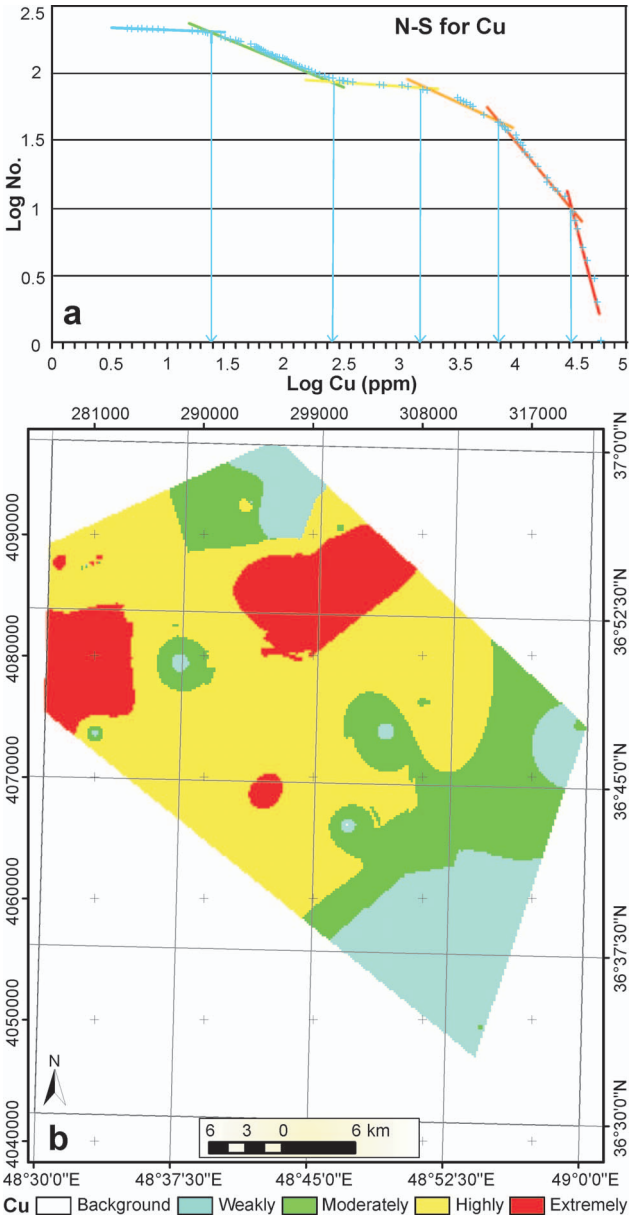

Fig. 5. a — Log-log plot of N-S method for Cu lithogeochemical data. **b** — Cu lithogeochemical population distribution map based on the N-S model.

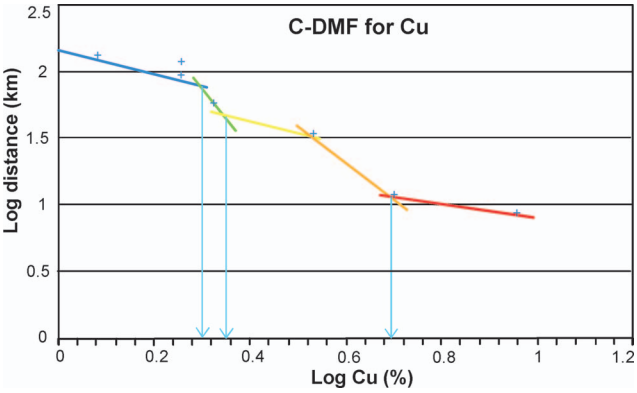

Fig. 6. Log-log plot from C-DMF model.

Application of N-S fractal method in lithogeochemical data analysis

After analysis of the stream sediment data, lithogeochemical samples were collected in the anomalous domains in the central and northern parts of the area (Fig. 3). The N-S log-log plot for Cu show there are six geochemical groups, as shown in Fig. 5. Extreme Cu anomalies start at 3.16 % Cu and are located in the central parts of the Tarom sheet. Additionally, anomalous domains derived via stream sediments were correlated with lithogeochemical extreme anomalies in the center of the area. High Cu anomalies (0.8–3.16 %) were situated in the central and NW parts of the area (Fig. 5).

Table 2: Average Cu grades of known mines and their distance to the major faults.

Copper mines, Name	Cu (%)	Distance to major fault (km)
Valider	9	8.5
Geligeh	2.2	15.6
Sorkh	1.2	14.3
Nughl Abad	2	19.6
Kale Kash	3.38	21.8
Lohneh	1.8	15.3
Qeshlaq	2.1	8.5
Shilandar	1.8	22.8
Amirabad	5	3
Kuhian	1	15.5

Table 3: Extreme and high geochemical anomalous areas and their distances to major faults in the Tarom sheet.

Cu stream sediment anomalies (ppm)	Distance to major fault (km)	Cu lithogeochemical anomalies (%)	Distance to major fault (km)
355	1.98	5.6	10.4
355	7.6	2	7.2
355	6.95	2	9.1
355	6.29	1.5	10.8

Application of Concentration-Distance to Major Fault fractal model

By means of C-DMF fractal modelling, six geochemical groups were separated based on the existence of known copper mines in the Tarom 1:100,000 sheet, as shown in Table 2. The log-log plot illustrates there are two major phases for Cu mineralization which have a multifractal character (Fig. 6). Copper mines with enrichment mineralization have Cu values higher than 2.2 %. The mines are located at distances less than 10 km from major faults (Table 3). The results indicate there is a relationship between the increasing of the copper mine grades and decreasing of the distance between the major faults and the copper mines in the area.

Geochemical anomalies identified by stream sediments and lithogeochemical data were used to validate the C-DMF model's results. All extreme Cu anomalies based on lithogeochemical data (Cu > 3.16 %) derived via stream sediments have a distance less than 8 km to the major faults. Moreover, all Cu extreme (Cu > 3.16 %) and high (0.8 < Cu < 3.16 %) anomalies based on lithogeochemical data occur at distances less than 11 km from major faults. Overall, the geochemical anomalies confirmed the results from the C-DMF fractal model.

Conclusion

Fractal/multifractal modelling is an effective instrument to separate mineralized zones. Application of the C-DMF model in the Tarom 1:100,000 sheet reveals that the main copper mineralizations are strongly correlated with their distance to the major faults in the studied area. The distances of known copper mineralizations with Cu values higher than 2.2 % to major faults are less than 10 km showing a positive correlation between Cu mineralization and the tectonic events. Moreover, major faults have played the main roles in hydrothermal fluids flow and the copper mineralization in the area. Based on the results, the C-DMF fractal modelling can be utilized for the reconnaissance and prospecting of magmatic and hydrothermal deposits.

Acknowledgment: The authors are grateful to Mr. Beighi, Mr. Rahbar and Mr. Haghigat, Exploration Department of Zanjan Province Industry, Mine and Trade Organization of Iran and Pars Peyazma Consulting Engineering Company for their sincere help and valuable discussions. We gratefully acknowledge the review of the anonymous referees for their constructive comments and suggestions. The careful editorial handling and cheerful encouragement by Assistant Editor Igor Petrík and Technical Editor Eva Petríková are gratefully appreciated.

References

Afzal P., Khakzad A., Moarefvand P., Rashidnejad Omran N., Esfandiari B. & Fadakar A.Y. 2010: Geochemical anomaly separation by multifractal modeling in Kahang (Gor Gor) porphyry system, Central Iran. *J. Geochem. Explor.* 104, 34–46.

Afzal P., Fadakar A.Y., Khakzad A., Moarefvand P. & Rashidnejad Omran N. 2011: Delineation of mineralization zones in porphyry Cu deposits by fractal concentration–volume modeling. *J. Geochem. Explor.* 108, 220–232.

Agterberg F.P., Cheng Q. & Wright D.F. 1993: Fractal modeling of mineral deposits. In: Elbrond J. & Tang X. (Eds.): 24th APCOM Sym. Proc., Montreal, Canada, 43–53.

Agterberg F.P. 1995: Multifractal modeling of the sizes and grades of giant and supergiant deposits. *Int. Geol. Rev.* 37, 1–8.

Agterberg F.P., Cheng Q., Brown A. & Good D. 1996: Multifractal modeling of fractures in the Lac du Bonnet Batholith, Manitoba. *Comput. Geosci.* 22, 5, 497–507.

Aichler J., Malec J., Večeřa J., Hanžl P., Buriánek D., Sidorinová T., Táborský Z., Bolormaa K. & Byambasuren D. 2008: Prospection for gold and new occurrences of gold-bearing mineralization in the eastern Mongolian Altay. *J. Geosci.* 53, 2, 123–138.

Amini B., Amini Chehragh M., Hirayama K. & Stoklin J. 1969: Geological map of Tarom, GSI, Tehran.

Arian M. 2011: Basement tectonics and geology of Iran. *Asar Nafis Press*, Tehran, 140–147 (in Persian).

Arian M., Maleki Z. & Noroozpour H. 2011: Cenozoic diastrophism and deformational events in the East-Central Alborz. *J. Basic Appl. Sci. Res.* 1, 2394–2400.

Azizi H., Tarverdi M.A. & Akbarpour A. 2010: Extraction of hydrothermal alterations from ASTER SWIR data from east Zanjan, northern Iran. *Adv. Space Res.* 46, 99–109.

Craw D. & Campbell J.R. 2004: Tectonic and structural setting for active mesothermal gold vein systems, Southern Alps, New Zealand. *J. Struct. Geol.* 26, 995–1005.

Cheng Q., Agterberg F.P. & Ballantyne S.B. 1994: The separation of geochemical anomalies from background by fractal methods. *J. Geochem. Explor.* 51, 109–130.

Cheng Q. 1999: Spatial and scaling modelling for geochemical anomaly separation. *J. Geochem. Explor.* 65, 3, 175–194.

Cheng Q. 2007: Mapping singularities with stream sediment geochemical data for prediction of undiscovered mineral deposits in Gejiu, Yunnan Province, China. *Ore Geol. Rev.* 32, 314–324.

Cheng Q. & Agterberg F.P. 2009: Singularity analysis of ore-mineral and toxic trace elements in stream sediments. *Comp. & Geosci.* 35, 234–244.

Deng J., Wang Q., Yang L., Wang Y., Gong Q. & Liu H. 2010: Delineation and explanation of geochemical anomalies using fractal models in the Heqing area, Yunnan Province, China. *J. Geochem. Explor.* 105, 95–105.

Fletcher W.K. 1997: Stream sediment geochemistry in today's exploration world. In: Proceeding of exploration 97. 4th Decennial Int. Conf. Min. Explor., Gubins, A.G., Editor, 249–260.

Gonçalves M.A., Mateus A. & Oliveira V. 2001: Geochemical anomaly separation by multifractal modeling. *J. Geochem. Explor.* 72, 91–114.

Grunsky E.C. & Smee B.W. 1999: The differentiation of soil types and mineralization from multi-element geochemistry using multivariate methods and digital topography. *J. Geochem. Explor.* 67, 287–299.

Gumiel P., Sanderson D.J., Arias M., Roberts S. & Martín-Izard A. 2010: Analysis of the fractal clustering of ore deposits in the Spanish Iberian Pyrite Belt. *Ore Geol. Rev.* 38, 307–318.

Harris J.R., Wilkinson L. & Grunsky E.C. 2000: Effective use and interpretation of lithogeochemical data in regional mineral exploration programs: application of Geographic Information Systems (GIS) technology. *Ore Geol. Rev.* 16, 107–143.

Hawkes R.A.W. & Webb H.E. 1979: Geochemistry in mineral exploration. 2nd Ed. *Acad. Press*, New York, 657.

Karimzadeh Somarin A. 2006: Geology and geochemistry of the

Mendejin plutonic rocks, Mianeh, Iran. *J. Asian Earth Sci*. 27, 819–834.

Li C., Xu Y. & Jiang X. 1994: The fractal model of mineral deposits. *Geol. Zhejiang* 10, 25–32 (in Chinese with English abstract).

Li C., Ma T. & Shi J. 2003: Application of a fractal method relating concentrations and distances for separation of geochemical anomalies from background. *J. Geochem. Explor*. 77, 167–175.

Mandelbrot B.B. 1983: The fractal geometry of nature. *Freeman*, San Fransisco, 1–468.

Micklethwaite S., Sheldon H.A. & Baker T. 2010: Active fault and shear processes and their implications for mineral deposit formation and discovery. *J. Struct. Geol*. 32, 151–165.

Monecke T., Monecke J., Herzig P.M., Gemmell J.B. & Monch W. 2005: Truncated fractal frequency distribution of element abundance data: a dynamic model for the metasomatic enrichment of base and precious metals. *Earth Planet. Sci. Lett*. 232, 363–378.

Mousavi S.R. 2012: Theory and modified rules to determine uncertainty in mineral prospection. *PhD. Dissertation*, TU Clausthal, 1–120.

Pereira H.G., Renca S. & Saraiva J. 2003: A case study on geochemical anomaly identification through principal components analysis supplementary projection. *Appl. Geochem*. 18, 37–44.

Reimann C., Filzmoser P. & Garrett R.G. 2005: Background and threshold: critical comparison of methods of determination. *Sci. Total Environ*. 346, 1–16.

Sadeghi B., Moarefvand P., Afzal P., Yasrebi A.B. & Daneshvar Saein L. 2012: Application of fractal models to outline mineralized zones in the Zaghia iron ore deposit, Central Iran. *J. Geochem. Explor*. 122, 9–19.

Sanderson D.J., Roberts S. & Gumiel P. 1994: A fractal relationship between vein thickness and gold grade in drill core from La Codosera, Spain. *Econ. Geol*. 89, 168–173.

Shi J. & Wang C. 1998: Fractal analysis of gold deposits in China: implication for giant deposit exploration. *Earth Sci. J. China Univ. Geosci*. 23, 616–618 (in Chinese with English abstract).

Tukey J.W. 1977: Exploratory data analysis. *First Ed. Pearson*, 1–688.

Turcotte D.L. 1996: Fractals and chaos in geophysics. 2nd Ed. *Camb. Univ. Press*, Cambridge, UK, 81–99.

Turcotte D.L. 1997: Fractals and chaos in geology and geophysics. *Camb. Univ. Press*, Cambridge, 1–416.

Turcotte D.L. 2002: Fractals in petrology. *Lithos* 65, 261–271.

Wang W., Zhao J., Cheng Q. & Liu J. 2012: Tectonic-geochemical exploration modeling for characterizing geo-anomalies in southeastern Yunnan district, China. *J. Geochem. Explor*. 122, 71–80.

Xu Y. & Cheng Q. 2001: A fractal filtering technique for processing regional geochemical maps for mineral exploration. *Geochem. Explor. Environ. Anal*. 1, 147–156.

Yasrebi A.B., Afzal P., Wetherelt A., Foster P. & Esfahanipour R. 2013: Correlation between geology and concentration-volume fractal models: significance for Cu and Mo mineralized zones separation in the Kahang porphyry deposit (Central Iran). *Geol. Carpathica* 64, 2, 153–163.

Zhao P. 1999: Theory and practice of geoanomaly in mineral exploration. 1st Ed. *China Univ. Geosci. Press*, Wuhan, China, 1–150 (in Chinese with English abstract).

Zuo R., Cheng Q. & Xia Q. 2009: Application of fractal models to characterization of vertical distribution of geochemical element concentration. *J. Geochem. Explor*. 102, 1, 37–43.

Zuo R. 2011: Identifying geochemical anomalies associated with Cu and Pb-Zn skarn mineralization using principal component analysis and spectrum-area fractal modeling in the Gangdese Belt, Tibet (China). *J. Geochem. Explor*. 111, 13–22.